

Supporting Information for “Deterministic loading of microwaves onto an artificial atom using a time reversal waveform”

Wei-Ju Lin^{†,1}, Yong Lu^{†,* ,2,3}, Ping Yi Wen^{†,4}, Yu-Ting Cheng,¹ Ching-Ping Lee,¹ Kuan Ting Lin,⁵ Kuan Hsun Chiang,⁶ Ming Che Hsieh,¹ Ching-Yeh Chen,¹ Chin-Hsun Chien,¹ Jia Jhan Lin,¹ Jeng-Chung Chen,^{1,7} Yen Hsiang Lin,^{1,7} Chih-Sung Chuu,^{1,7} Franco Nori,^{8,9} Anton Frisk Kockum,² Guin Dar Lin,^{5,10,11} Per Delsing,² and Io-Chun Hoi^{*,12,1}

¹*Department of Physics, National Tsing Hua University, Hsinchu 30013, Taiwan*

²*Department of Microtechnology and Nanoscience (MC2),*

Chalmers University of Technology, SE-412 96 Gothenburg, Sweden

³*3rd Institute of Physics, IQST, and Research Centre SCoPE, University of Stuttgart, Stuttgart, Germany*

⁴*Department of Physics, National Chung Cheng University, Chiayi 621301, Taiwan*

⁵*CQSE, Department of Physics, National Taiwan University, Taipei 10617, Taiwan*

⁶*Department of Physics, National Central University, Jhongli, 32001, Taiwan*

⁷*Center for Quantum Technology, National Tsing Hua University, Hsinchu 30013, Taiwan*

⁸*Theoretical Quantum Physics Laboratory, RIKEN Cluster for Pioneering Research, Wako-shi, Saitama 351-0198, Japan*

⁹*Physics Department, The University of Michigan, Ann Arbor, Michigan 48109-1040, USA*

¹⁰*Physics Division, National Center for Theoretical Sciences, Taipei 10617, Taiwan*

¹¹*Trapped-Ion Quantum Computing Laboratory, Hon Hai Research Institute, Taipei 11492, Taiwan*

¹²*Department of Physics, City University of Hong Kong,*

Tat Chee Avenue, Kowloon, Hong Kong SAR, China

(Dated: September 29, 2022)

CONTENTS

S1. Experimental setup and device	1
S2. Steady-state reflection coefficient for extracting parameters of the qubits	3
S3. Full data for loading coherent photons with exponentially rising waveforms onto a qubit	4
S4. Loading a weak coherent state onto a qubit with other waveforms	9
S5. Discussion on optimal loading efficiency and optimal symmetry factor	9
S6. General formalism for a single-photon pulse (Fock state)	9
S7. Output field and loading efficiency	10
S8. Loading a single-photon Fock state using an exponentially rising waveform	12
S9. Time-reversal symmetry for Fock-state input	15
References	16

S1. EXPERIMENTAL SETUP AND DEVICE

Figure S1 shows the experimental setups for samples 1 and 2. In both samples, transmon qubits are coupled to a semi-infinite one-dimensional (1D) transmission line with characteristic impedance $Z_0 \simeq 50 \Omega$. Arbitrary waveform generators (AWGs) shape the waveform of input coherent photons, while digitizers capture the reflected signal, enabling us to resolve the time dynamics of the qubit and the photons.

[†] W. -J. L, Y. L and P. Y. W contributed equally to this work.

[*] I.-C. Hoi (iochoi@cityu.edu.hk), Y. Lu (kdlyong@outlook.com)

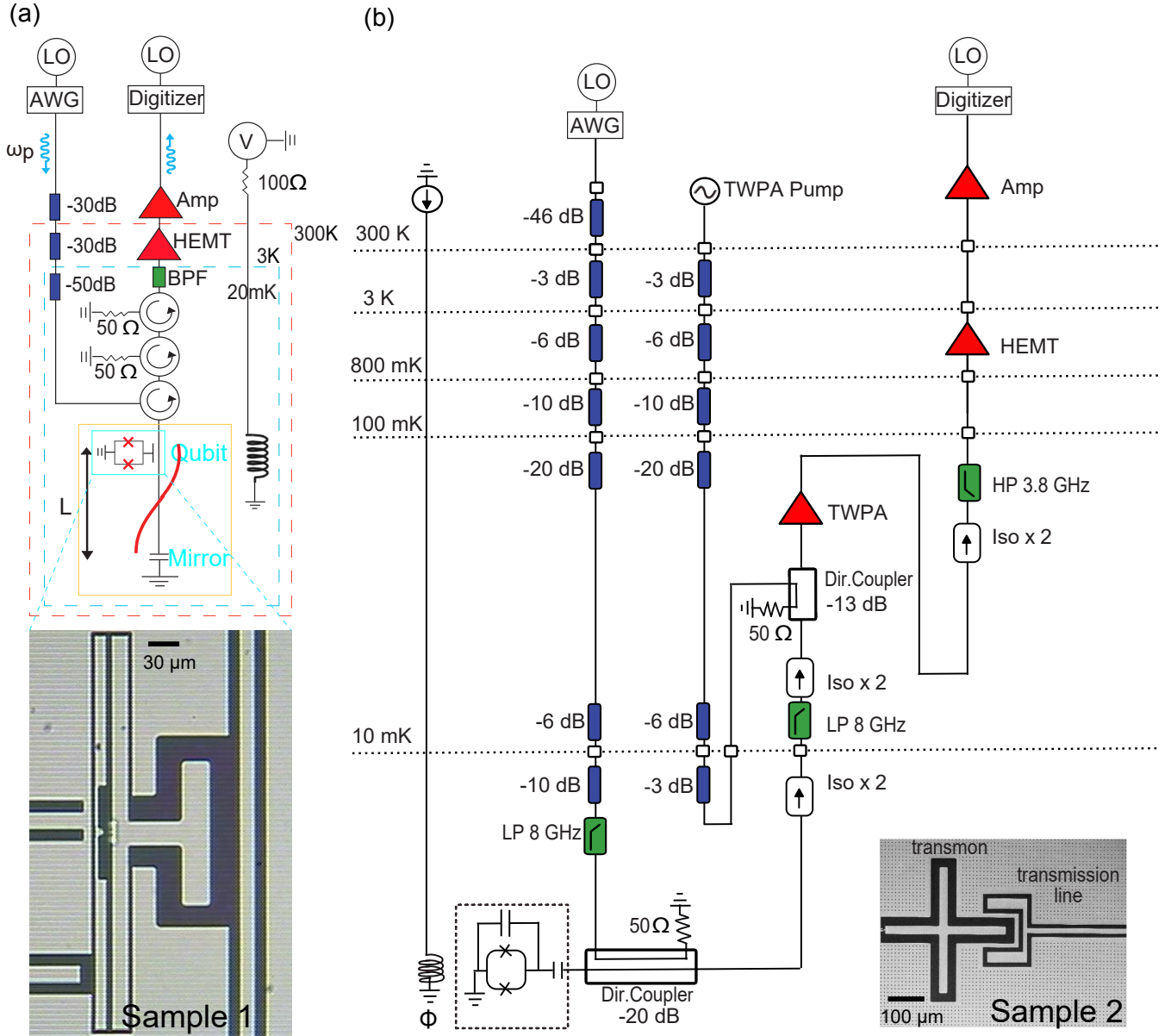


Figure S1. Photos of our devices and sketches of the experimental setups. (a) Measurement setup for sample 1. In the device image, shown in the zoom-in at the bottom, the two long bright parts form the qubit capacitance, and the extended pad from the one on the right determines the relatively weak capacitive coupling to the transmission line. Two Josephson junctions form a superconducting quantum interference device (SQUID) loop between the two islands forming the qubit capacitance. In the sketch of the setup, the red curve represents the electromagnetic field distribution along the transmission line. The qubit is placed $L \simeq 12$ mm from the mirror (capacitance to ground at the end of the transmission line). For the qubit frequency $\omega_{10}/2\pi = 4.85$ GHz, the location corresponds to 0.65λ . The roundtrip time from the qubit to the mirror and back, $2L/v \sim 0.2$ ns, is small compared to the timescale of the atomic evolution, T_2 . A superconducting coil controlled by a dc voltage V induces a global magnetic field and enables us to tune the qubit frequency ω_{10} . For measurements, coherent signals at frequency ω_p are synthesized at room temperature and fed through attenuators (blue rectangles) to the sample, which resides in a cryostat cooled to 20 mK to avoid thermal fluctuations affecting the experiment. The reflected signal passes circulators, filters (green rectangle), and amplifiers (red triangles), and is then collected by the digitizer. (b) Measurement setup of sample 2. In the device image, shown in the zoom-in in the lower right, the bright cross forms the qubit capacitance. A SQUID loop with two Josephson junctions connects to the left piece of the cross, while the transmission line couples to the qubit through the right piece of the cross. The measurement scheme is similar to (a) except for the inclusion of a travelling-wave parametric amplifier (TWPA), which leads to a noise level V_N about two times smaller than in sample 1 and smaller uncertainty in extracted qubit parameters.

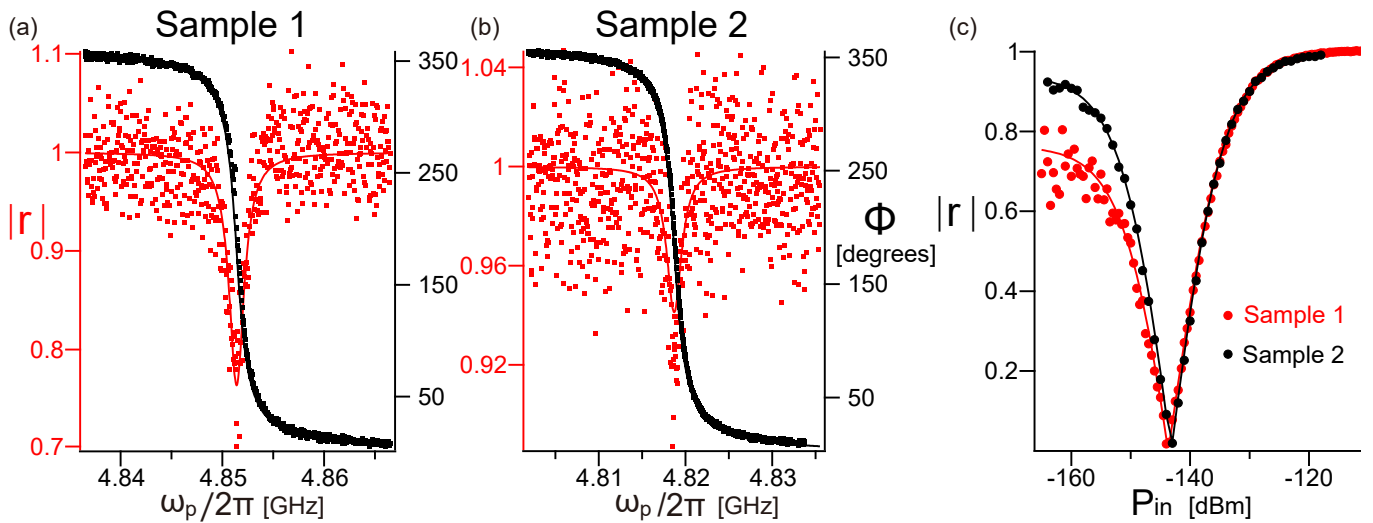


Figure S2. Steady-state reflection measurement with a continuous coherent probe. (a, b) Measured magnitude $|r|$ (red dots) and phase Φ (black dots) of $r = |r|e^{i\Phi}$ as a function of probe frequency ω_p with a probe power of -166 dBm for samples 1 and 2, respectively. Theoretical fits (solid curves) give us the values of Γ , γ , and ω_{10} mentioned in the main text. (c) Measured magnitude response $|r|$ as a function of the incident resonant power P_{in} for samples 1 (red dots) and 2 (black dots). The theoretical fits (solid curves) yield the atom-field coupling k mentioned in the main text.

S2. STEADY-STATE REFLECTION COEFFICIENT FOR EXTRACTING PARAMETERS OF THE QUBITS

In this section, we describe how we extract the parameters of the qubit from data obtained in the steady-state reflection measurements. The reflection coefficient for a continuous weak probe is given by [S1]

$$r = 1 - \frac{\Gamma}{\gamma + i\delta\omega_p}, \quad (\text{S1})$$

where Γ is the qubit relaxation rate, γ is the qubit decoherence rate $1/T_2$, and $\delta\omega_p = \omega_{10} - \omega_p$. We apply a weak probe with a power of -166 dBm and measure the reflection coefficient of the two samples. The results are shown in Fig. S2(a)-(b). The solid curves (both magnitude and phase) in Fig. S2(a)-(b) are fits to the data using Eq. (S1) and the circle fit technique in Ref. [S2]. This allows us to extract values for Γ , γ , and ω_{10} .

For a resonant probe, the reflection coefficient is given by [S1]

$$r = 1 - \frac{\Gamma^2}{\Gamma\gamma + \Omega_p^2}, \quad (\text{S2})$$

where Ω_p is the Rabi frequency of the probe. In Fig. S2(c), we show the measured magnitude of the reflection coefficient as a function of resonant input power P_{in} . The nonlinear power dependence allows us to extract k in $\Omega_p = k\sqrt{P_{in}}$ using Eq. (S2).

This nonlinear power dependence can be used to calibrate the absolute power P_{in} . The calibration is done by finding the critical power $P_{in} = \hbar\omega_{10}\Gamma/8$, assuming negligible pure dephasing, where coherent emission is perfectly suppressed, i.e., $|r| = 0$ [S3].

We calculate $\Gamma_{\phi,n}$ from Γ and γ , using $\gamma = 1/T_2 = \Gamma/2 + \Gamma_{\phi,n}$, where $\Gamma_{\phi,n} = \Gamma_n/2 + \Gamma_\phi$ with the pure dephasing rate Γ_ϕ and nonradiative decay Γ_n . Note that Γ_ϕ and Γ_n can be further separated different contributions as in [S2]. We expect that $\Gamma_{\phi,n}$ is dominated by the pure dephasing rate since the same fabrication process as in [S3] was used where the non-radiative decay is negligible. We calculate T_2 from γ .

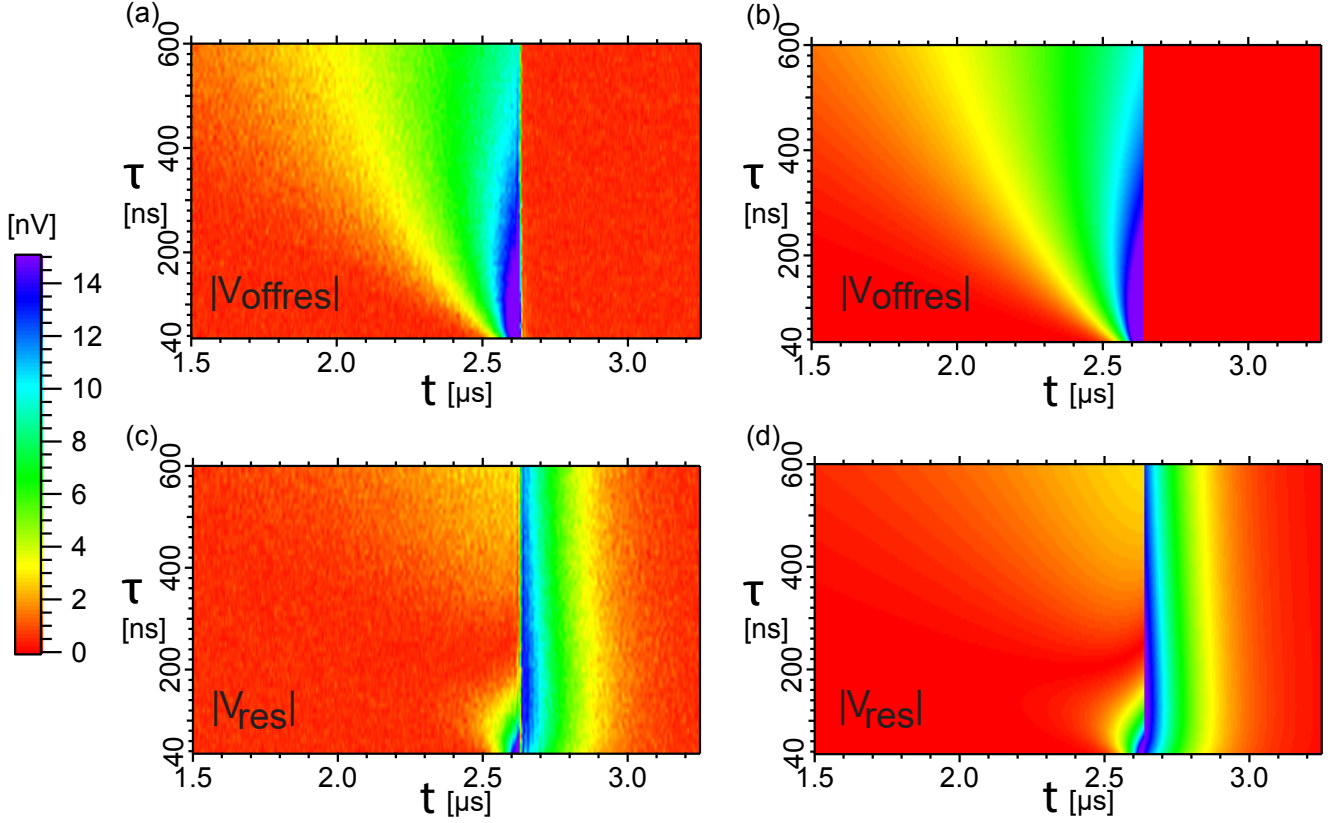


Figure S3. Magnitude of the reflected field for sample 1 when driven with an exponentially rising input coherent pulse with $N = 0.09$. (a, c) The experimental data of the reflected field with the qubit far off resonance, $|V_{\text{offres}}|$, and on resonance, $|V_{\text{res}}|$, respectively. (b, d) Theory simulations of the data in panels (a) and (c), respectively. The simulations are performed using the parameters extracted from Fig. S2 (no free parameters). The agreement between the data and the simulations is excellent.

S3. FULL DATA FOR LOADING COHERENT PHOTONS WITH EXPONENTIALLY RISING WAVEFORMS ONTO A QUBIT

In this section, we present the full data of Fig. 2 and Fig. 3 in the main text. To obtain the output, we further use the calibrated gain of the amplifiers, which is about 68 dB for sample 1 and 99 dB for sample 2. This is because that we know the absolute power at the critical point at the sample, and we know the power at the critical point at the digitizer at room temperature, so we can calibrate the gain. Figure S3 shows the magnitude of the reflected field as a function of characteristic time τ and time t when the input field has the number of photons contained in the pulse $N = 0.09$. This is the data from which we calculate the loading efficiency η and symmetry factor S in Fig. 2(b)-(c). Figure S4 shows a magnification in Fig. 2a. Figure S5 shows step by step how the raw data in Fig. S3(a,c) was converted to the values in Fig. 2(b)(c) for $\tau = 140$ ns. In experiment, due to the finite sampling resolution and in order to obtain more accurate values of S and η , we use the definitions

$$\eta = \frac{\int_{t_0^{\text{res}}}^{t_f} [|V_{\text{res}}(t)| - |V_N|]^2 dt}{\int_{t_i}^{t_0^{\text{offres}}} [|V_{\text{offres}}(t)| - |V_N|]^2 dt}, \quad (\text{S3})$$

$$S = \frac{\int_{t_i}^{t_0^{\text{offres}}} [|V_{\text{offres}}(t)| - |V_N|][|V_{\text{res}}(2t_0 - t)| - |V_N|] dt}{\int_{t_i}^{t_0^{\text{offres}}} [|V_{\text{offres}}(t)| - |V_N|]^2 dt}, \quad (\text{S4})$$

where t_0^{offres} and t_0^{res} are slightly different. In the ideal case, where the time resolution is zero, we have $t_0^{\text{res}} = t_0^{\text{offres}}$. To simplify the formulas, we therefore use $t_0 = t_0^{\text{offres}} = t_0^{\text{res}}$ for the definition of S and η in the main text. The values of the different times appearing in Eqs. (S3) and (S4) are given in Table S1. Note that V_{offres} is the reflected voltage amplitude when the qubit is far detuned. The incoming voltage field will be fully reflected by the mirror and therefore the reflected voltage is the same as the incoming field. V_{res} is the reflected voltage amplitude when the qubit is on

Time	t_0^{res}	t_0^{offres}	$t_0 = (t_0^{\text{res}} + t_0^{\text{offres}})/2$	t_f	t_i
μs	2.64	2.62	2.63	3.2	2.1

Table S1. Times used in the integrals in Fig. S5, Eq. (S3), and Eq. (S4).

resonance. The detection of these signals is based on heterodyne detection. Since there is a π phase shift between V_{offres} and V_{res} , we use the absolute sign to rule out the change of the phase and ensure positive value of symmetry factor S .

Figure S6 shows the magnitude of the reflected field for different N from 0.0004 to 4.12, but with the same characteristic time τ of 145 ns. This is the data from which we calculate the loading efficiency η and symmetry factor S in Fig. 3(a)-(b).

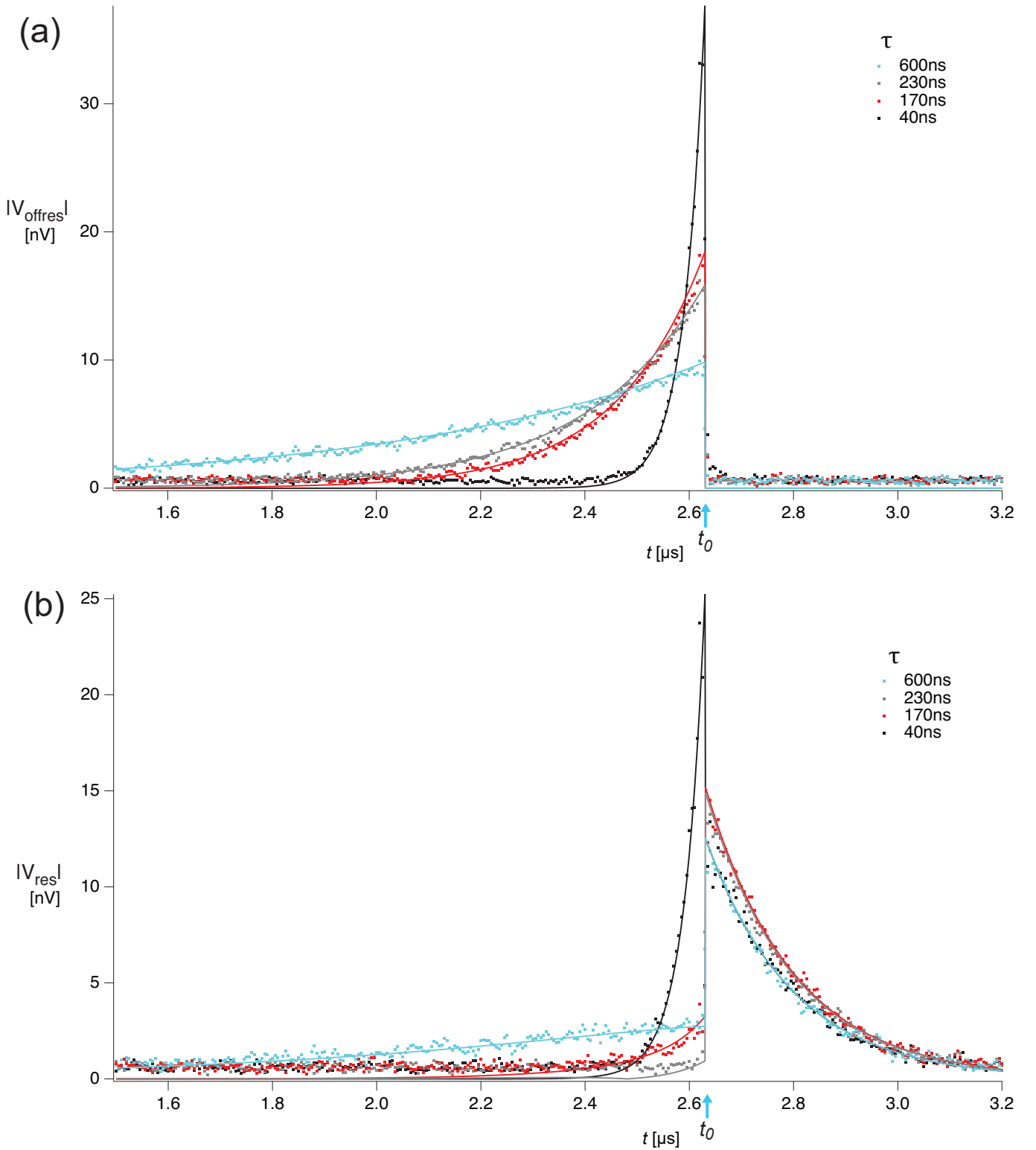


Figure S4. The magnification in Fig. 2a in the main text. The experimental data of the reflected field with (a) the qubit far off resonance, $|V_{\text{offres}}|$, and (b) on resonance, $|V_{\text{res}}|$, respectively. The agreement between the data and the simulations is excellent. When the pulse is on, destructive interference between the qubit emission and the reflected input field suppresses the output. Nearly perfect interference between input and qubit emission is observed for $\tau = 230$ ns. After the pulse is turned off, the atom emits a coherent field. The amount of emitted field depends on τ . Before t_0 , the incoming field has an exponentially rising shape. For τ far away from T_2 , such as 40 ns and 600 ns, the emitted field does not interfere perfectly destructively with the incoming field, leading to significant increasing signal before t_0 .

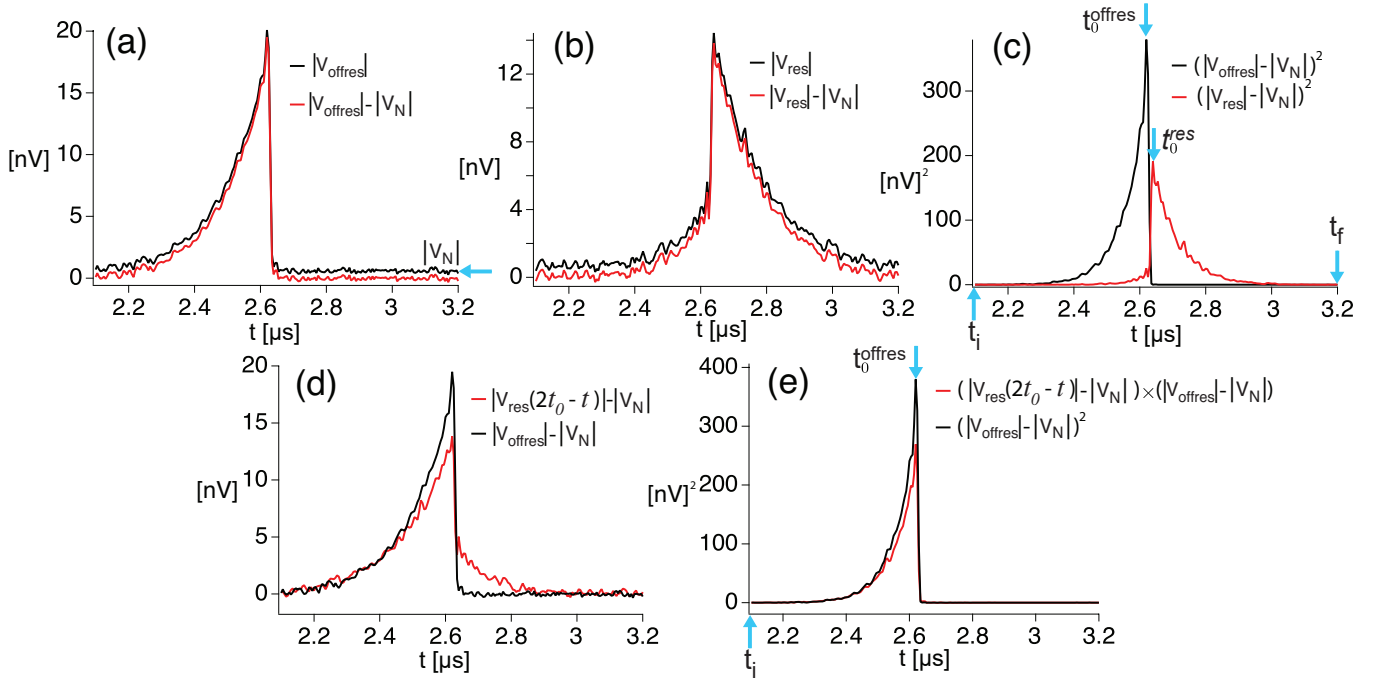


Figure S5. The steps for converting the raw data in Fig. S3(a,c) to the values in Fig. 2(b,c) at $\tau = 140$ ns. (a) Raw data V_{offres} for the incoming exponential rising pulse and the result $|V_{\text{offres}}| - |V_N|$ after subtracting the noise floor V_N . (b) Raw data $|V_{\text{res}}|$ of the reflected coherent photons when the input pulse is on resonance with the qubit, and the result $|V_{\text{res}}| - |V_N|$ after subtracting the noise. (c) Next, we square the voltages from panels (a) and (b), respectively, which yields a result proportional to power. The loading efficiency η is the emission energy divided by the incoming energy, which is the area under $(|V_{\text{res}}| - |V_N|)^2$ between t_0^{res} and t_f divided by the area under $(|V_{\text{offres}}| - |V_N|)^2$ between t_i and t_0^{offres} , as defined in Eq. (S3). (d) Time reverse of the emitted field $|V_{\text{res}}(2t_0 - t)| - |V_N|$ and the incoming field $|V_{\text{offres}}| - |V_N|$. (e) The product of the time reversed emitted field and the incoming field. The symmetry factor S is the area under $[|V_{\text{offres}}|(t) - |V_N|][|V_{\text{res}}(2t_0 - t)| - |V_N|]$ between t_i and t_0^{offres} divided by the area under $(|V_{\text{offres}}| - |V_N|)^2$ between t_i and t_0^{offres} , as defined in Eq. (S4).

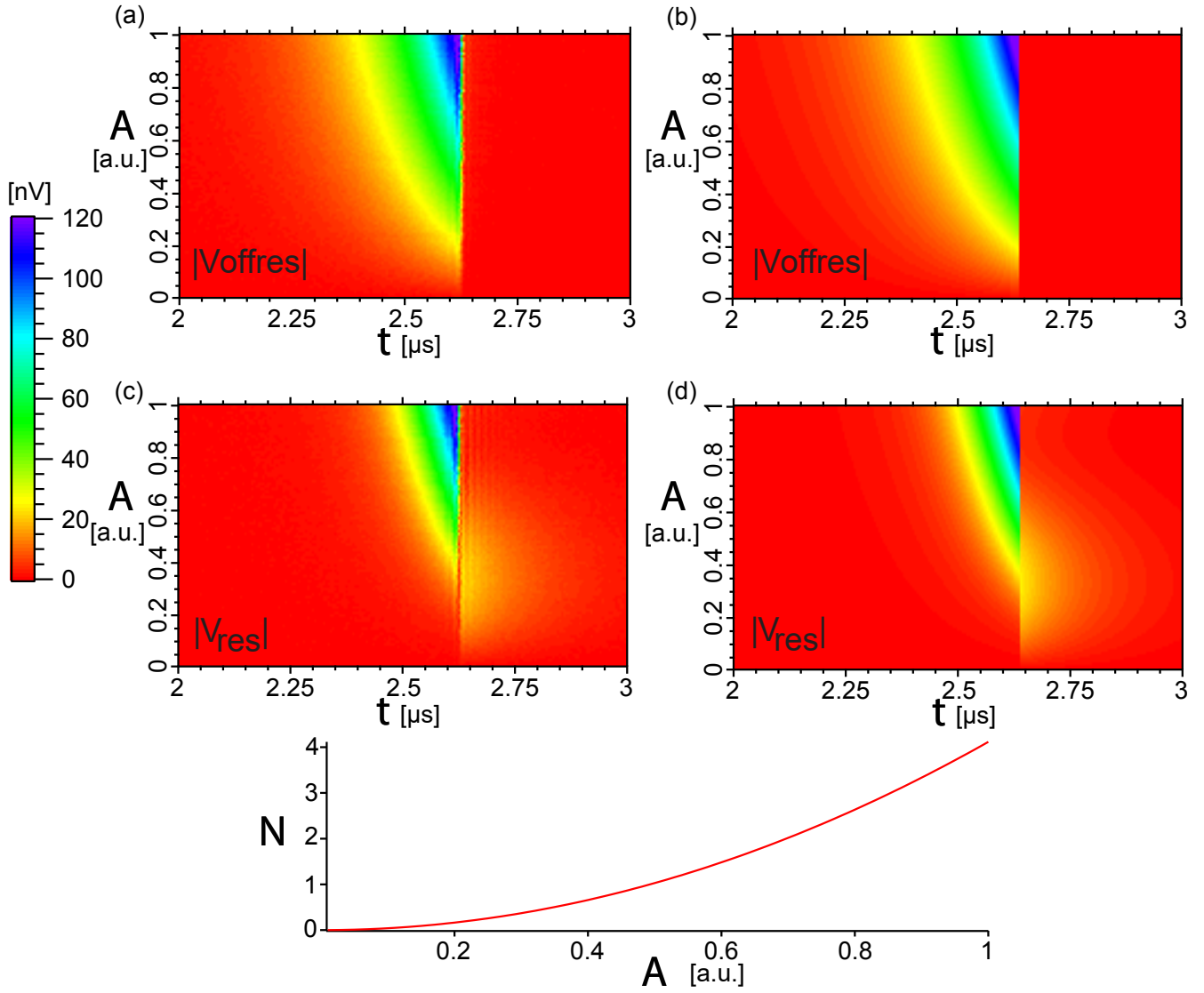


Figure S6. Magnitude of the reflected field for sample 1 when driven with an exponentially rising input coherent pulse with different N , but with the same characteristic time $\tau = 145$ ns. (a, c) The experimental data of the reflected field with the qubit far off resonance, $|V_{\text{offres}}|$, and on resonance, $|V_{\text{res}}|$, respectively. (b, d) Theory simulations of the data in panels (a) and (c), respectively. The simulations are performed using the parameters extracted from Fig. S2 (no free parameters). The agreement between the data and the simulations is excellent. (e) The relation between N and amplitude A in panels (a)-(d), where A is given in arbitrary units. With a high-power resonant drive, the atom will increase incoherent scattering, and decrease coherent scattering, leading to low loading efficiency.

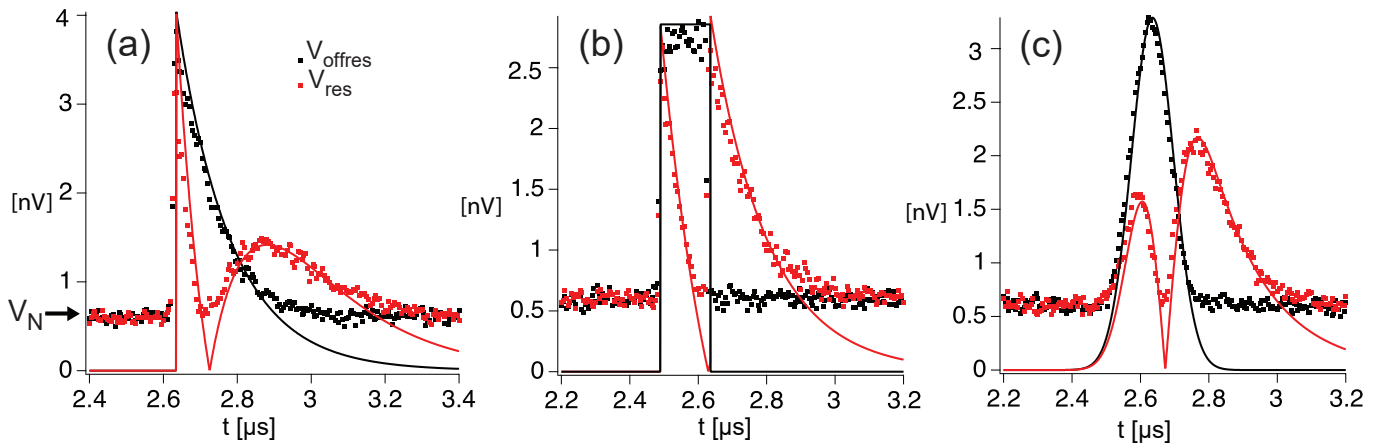


Figure S7. Loading a weak coherent state onto the qubit of sample 1 with other pulse shapes, all with $N = 0.004$. In all plots, black and red represents input (off-resonant) and output (resonant), respectively. Experimental data are shown as square markers; each trace is averaged over 450 million runs. Solid curves are theoretical calculations. (a) Exponentially decaying pulse with characteristic time 145 ns. (b) Square pulse with width 145 ns. (c) Gaussian pulse with full width at half maximum 145 ns.

Sample	E_C/h	E_J/h	E_J/E_C
Units	[MHz]	[GHz]	-
1	385	8.9	23
2	200	15.7	78

Table S2. From the two-tone spectroscopy, we extract the anharmonicity, which approximately equals the charging energy E_C of the transmon qubits. We calculate the Josephson energy E_J and E_J/E_C from $\omega_{10} \simeq \sqrt{8E_J E_C} - E_C$.

S4. LOADING A WEAK COHERENT STATE ONTO A QUBIT WITH OTHER WAVEFORMS

For comparison, we study different input pulse shapes with the same N for sample 1: exponentially decaying, square, and Gaussian. In Fig. S7(a), we show the exponentially decaying waveform, whose power spectrum is the same as for the exponentially rising pulse. The incoming wave and emitted wave interfere, leading to distortion of the waveform. For the square pulse in Fig. S7(b), the loading efficiency is 47.4%, which is 17% lower than for the exponentially rising pulse (64.4%). For the Gaussian pulse in Fig. S7(c), the output splits into two peaks. For exponentially decaying waveform and Gaussian waveform, since there is no clear time separation between absorption and emission, the loading efficiency cannot be well defined.

S5. DISCUSSION ON OPTIMAL LOADING EFFICIENCY AND OPTIMAL SYMMETRY FACTOR

Assuming a weak drive $\Omega \ll \gamma$, with optimal mode matching $1/\tau = \gamma$, according to Eq. (8) in the main text, we have the maximal value of loading efficiency $\eta = (1 + 2\Gamma_{\phi,n}/\Gamma)^{-2}$ and the maximal value of symmetry factor $S = (1 + 2\Gamma_{\phi,n}/\Gamma)^{-1}$. This was demonstrated using sample 1. To further increase S and η , in particular, when $\Gamma \gg \Gamma_{\phi,n}$, both the loading efficiency and the symmetry factor reach unity. Sample 2 achieved this by having a high E_J/E_C ratio S2, which reduced charge noise, and thus the pure dephasing ($\Gamma_{\phi,n}/2\pi = 0.113$ MHz for sample 1; $\Gamma_{\phi,n}/2\pi = 0.031$ MHz for sample 2). As an outlook, keeping $\Gamma_{\phi,n}$ fixed, we can also decrease the ratio $\Gamma_{\phi,n}/\Gamma$ by increasing the coupling between the waveguide and the qubit, and thus increase S and η .

S6. GENERAL FORMALISM FOR A SINGLE-PHOTON PULSE (FOCK STATE)

The Hamiltonian describing a transmon qubit coupled to a semi-infinite 1D waveguide can be written as $H = H_S + H_B + H_{\text{int}}$, where we only consider the ground state and the first-excited state of the transmon. The bare qubit part $H_S = \hbar\omega_0\sigma_+\sigma_-$ and the field one $H_B = \int_0^\infty d\omega \hbar\omega a_\omega^\dagger a_\omega$, where $\sigma_+ = |e\rangle\langle g|$ and $\sigma_- = |g\rangle\langle e|$ are the ladder operators between the qubit ground state $|g\rangle$ and excited state $|e\rangle$ separated by the transition energy $\hbar\omega_0$; a_ω^\dagger

and a_ω are the field creation and annihilation operators, respectively, of mode ω . The photonic operators obey the commutation relation $[a_\omega, a_{\omega'}^\dagger] = \delta(\omega - \omega')$. Under the rotating-wave approximation, the interaction Hamiltonian reads

$$H_{\text{int}} = -i\hbar \int_0^\infty d\omega g(\omega) \cos(k_\omega x + \phi_0) \sigma_- a_\omega^\dagger + \text{H.c.}, \quad (\text{S5})$$

where $g(\omega)$ is the coupling strength at frequency ω , the wavenumber is $k_\omega = \omega/v_g$ with v_g the speed of light in the waveguide, and H.c. denotes Hermitian conjugate. Note that the cosine function in H_{int} reflects the formation of a standing wave when the transmission line is terminated by a mirror at $x = 0$ with a phase ϕ_0 depending on whether the mirror is capacitive or inductive. The phase $\phi_0 = 0$ ($\pi/2$) corresponds to an anti-node (a node) at $x = 0$.

The Heisenberg equations of motion of the atomic operators are given by [S4, S5]

$$\dot{\sigma}_z = -\Gamma(x)(\sigma_z + I) + 2 \int_0^\infty d\omega g(\omega) \cos(k_\omega x) \left(\tilde{\sigma}_+(t) a_\omega(0) e^{-i(\omega - \omega_0)t} + \text{H.c.} \right), \quad (\text{S6})$$

$$\dot{\tilde{\sigma}}_+ = -\gamma(x) \tilde{\sigma}_+ - \int_0^\infty d\omega g(\omega) \cos(k_\omega x) e^{i(\omega - \omega_0)t} a_\omega^\dagger(0) \sigma_z(t), \quad (\text{S7})$$

where we have used $\sigma_\pm = \tilde{\sigma}_\pm e^{\pm i\omega t}$ and looked at the slowly varying $\tilde{\sigma}_\pm$. The spontaneous decay rate of the qubit is given by $\Gamma(x) = \Gamma \cos^2(k_0 x) \equiv T_1^{-1}$ with $\Gamma = 2\pi g^2(\omega_0)$. The overall decoherence rate is $\gamma(x) = \Gamma(x)/2 + \Gamma_{\phi,n} \equiv T_2^{-1}$ with $\Gamma_{\phi,n}$ the sum of pure dephasing rate and non-radiative decay.

An arbitrary single-photon state can be expressed as

$$|1_p\rangle = \int_0^\infty d\omega g(\omega) \cos(k_\omega x) f(\omega) a_\omega^\dagger |0\rangle, \quad (\text{S8})$$

where $f(\omega)$ is the spectral distribution function [S4, S6, S7] and $|0\rangle$ denotes the multi-mode vacuum state. Then the initial state of the system can be written as a direct product state of the qubit ground state and a single-photon state $|\psi_0\rangle = |g, 1_p\rangle$. The evolution of the atomic variables can be obtained by solving

$$\langle g, 1_p | \dot{\sigma}_z | g, 1_p \rangle = -\Gamma(x) (\langle g, 1_p | \sigma_z | g, 1_p \rangle + 1) + 2\sqrt{\Gamma} \cos(k_0 x) [\xi(t) \langle g, 1_p | \tilde{\sigma}_+ | g, 0 \rangle + \xi^*(t) \langle g, 0 | \tilde{\sigma}_- | g, 1_p \rangle], \quad (\text{S9})$$

$$\langle g, 1_p | \dot{\tilde{\sigma}}_+ | g, 0 \rangle = -\gamma(x) \langle g, 1_p | \tilde{\sigma}_+ | g, 0 \rangle + \sqrt{\Gamma} \cos(k_0 x) \xi^*(t), \quad (\text{S10})$$

where

$$\xi(t) = \frac{\sqrt{\Gamma} \cos(k_0 x)}{2\pi} \int_0^\infty f(\omega) e^{-i(\omega - \omega_0)t} d\omega \quad (\text{S11})$$

represents the temporal waveform of the incident pulse, which should be properly normalized by $\int_{-\infty}^\infty |\xi(t)|^2 dt = 1$.

S7. OUTPUT FIELD AND LOADING EFFICIENCY

In this section, we define the efficiency of ‘‘loading a photon’’ given an incident pulse in the semi-infinite waveguide geometry. Following the standard input-output formalism, we have [S8, S9]

$$a_{\text{out}}(t) = a_{\text{in}}(t) - \sqrt{\Gamma} \cos(k_0 x) \tilde{\sigma}_-(t), \quad (\text{S12})$$

where the input and output operators are given by

$$a_{\text{in}}(t) = \frac{1}{\sqrt{2\pi}} \int_0^\infty d\omega a_\omega(0) e^{-i(\omega - \omega_0)t} \quad (\text{S13})$$

and

$$a_{\text{out}}(t) = \frac{1}{\sqrt{2\pi}} \int_0^\infty d\omega a_\omega(t_f) e^{-i(\omega - \omega_0)t} e^{i\omega t_f} \quad (\text{S14})$$

respectively. We calculate the input and output photon fluxes via

$$F_{\text{in}}(t) = \langle a_{\text{in}}^\dagger(t) a_{\text{in}}(t) \rangle, \quad (\text{S15})$$

and

$$F_{\text{out}}(t) = \left\langle a_{\text{out}}^\dagger(t) a_{\text{out}}(t) \right\rangle = F_{\text{in}}(t) + \Gamma(x) \langle \tilde{\sigma}_+ \tilde{\sigma}_- \rangle - \sqrt{\Gamma} \cos(k_0 x) \left(\langle \tilde{\sigma}_+ a_{\text{in}} \rangle + \left\langle a_{\text{in}}^\dagger \tilde{\sigma}_- \right\rangle \right). \quad (\text{S16})$$

The loading efficiency is then defined as

$$\eta = \frac{\int_{t_0}^{\infty} F_{\text{out}}(t) dt}{\int_{-\infty}^{\infty} F_{\text{in}}(t) dt}, \quad (\text{S17})$$

where t_0 refers to the end time of the loading pulse. The definition of loading efficiency and symmetry factor for the Fock-state photon is different from the coherent state, due to their distinct properties. This definition of efficiency captures the contribution of incoherent emission and directly reflects the excitation of the qubit. In our experiments with exponentially rising input pulses, t_0 is simply the time when the pulse is turned off: $t_0 = 0$. Note that this efficiency is nothing but the ratio of the emitted energy to the incident energy. In the following, we look at the case with a single-photon Fock state being fed in. The efficiency can be numerically computed by solving the dynamical Eqs. (S9)-(S10).

S8. LOADING A SINGLE-PHOTON FOCK STATE USING AN EXPONENTIALLY RISING WAVEFORM

Now we calculate the loading efficiency with an incident single-photon Fock state $|1_p\rangle$, $N=1$, which has the exponentially rising waveform

$$\xi(t) = \sqrt{2/\tau} e^{t/\tau} \Theta(-t) \quad (\text{S18})$$

with τ the characteristic time constant and

$$\Theta(t) = \begin{cases} 0 & t < 0 \\ 1 & t \geq 0 \end{cases} \quad (\text{S19})$$

the Heaviside step function. We assume that the qubit is placed at one of the antinodes $x = 2n\pi/k_0$ with $k_0 = \omega_0/v_g$ and n an integer. Following the approach summarized in the preceding sections, we obtain the input flux

$$F_{\text{in}}(t) = \frac{2}{\tau} e^{2t/\tau} \Theta(-t) \quad (\text{S20})$$

and the output flux

$$F_{\text{out}}(t) = \begin{cases} \left[1 - \frac{4\Gamma}{\tau(\gamma+1/\tau)(\Gamma+2/\tau)} \right] \frac{2e^{2t/\tau}}{\tau} & t < 0 \\ \frac{4\Gamma^2}{\tau(\gamma+1/\tau)(\Gamma+2/\tau)} e^{-\Gamma t} & t > 0 \end{cases} \quad (\text{S21})$$

with $\gamma = \Gamma/2 + \Gamma_{\phi,n}$. The corresponding loading efficiency is

$$\eta(\tau) = \frac{4\Gamma}{\tau(\gamma + 1/\tau)(\Gamma + 2/\tau)}. \quad (\text{S22})$$

It is expected that, for $t < 0$, the output signal is proportional to the input one with the second term inside the square bracket of Eq. (S21) accounting for the scattered contribution due to the qubit. Typical photon input/output curves are shown in Fig. S8. In order to maximize the loading efficiency, any output flux needs to be eliminated by perfect destructive cancellation between the input and scattered signals. This occurs only when $\tau = 2/\Gamma$ with $\Gamma_{\phi,n} = 0$, which corresponds to the exact time reversal of the spontaneous emission process and yields $\eta = 1$. For the general case with finite pure dephasing, the time constant yielding the highest efficiency is determined by $\tau_{\text{opt}} = \sqrt{2/(\gamma\Gamma)}$, slightly different from $\tau_{\text{opt}} = 1/\gamma$ in the coherent case discussed in the main text.

Now we discuss the effect of $\Gamma_{\phi,n}$ on the efficiency with single-photon Fock-state inputs. Panels (a) and (b) in Figs. S8, S9, and S11 compare two samples with different $\Gamma_{\phi,n}$. For each sample, we vary the characteristic time constant of the exponentially rising input pulse, as shown in Fig. S8, and find the optimal time constant τ_{opt} that maximizes the loading efficiency. In the first sample with $\Gamma_{\phi,n}/\Gamma \approx 7\%$, we find $\eta \approx 93.8\%$ owing to an observable F_{out} , interpreted as excitation loss, during the loading stage ($t < 0$). This loss is suppressed as $\Gamma_{\phi,n}/\Gamma$ decreases and we find $\eta \approx 98.5\%$ in the second sample with $\Gamma_{\phi,n}/\Gamma \approx 1.5\%$. Further, we observe, by comparing the curves of the same type of input in Fig. S9(a)-(b), that generally the loading efficiency is more robust against pure dephasing for Fock-state input than for coherent-state input.

Compared to a $N = 1$ coherent state with a Poisson distribution over the photon numbers, a single-photon Fock state only has a single photon ($N = 1$), leading to a much higher loading efficiency. If $\Gamma_{\phi,n} = 0$, the loading efficiency approaches unity both for coherent-state $N \ll 1$ and single-photon Fock-state ($N = 1$) pumping when perfect destructive interference between the input and the scattered field is realized during the loading process. However, the loading of a coherent state is less robust to dephasing than the loading of a single-photon Fock state. This is because a coherent state is a superposition of multiple Fock states with definite phase relations, which are more easily affected by dephasing, leading to a lower loading efficiency.

Figure S10(b) shows that the loading efficiency is a monotonic decreasing function of the $\Gamma_{\phi,n}$. For a large $\Gamma_{\phi,n}$, the efficiency can still be kept above 50% given an exponentially rising Fock-state input pulse, but becomes very poor for coherent-state input. Note that the optimized pulse profile also depends on the choice of input states. This can be seen from previous discussions and Fig. S10(a).

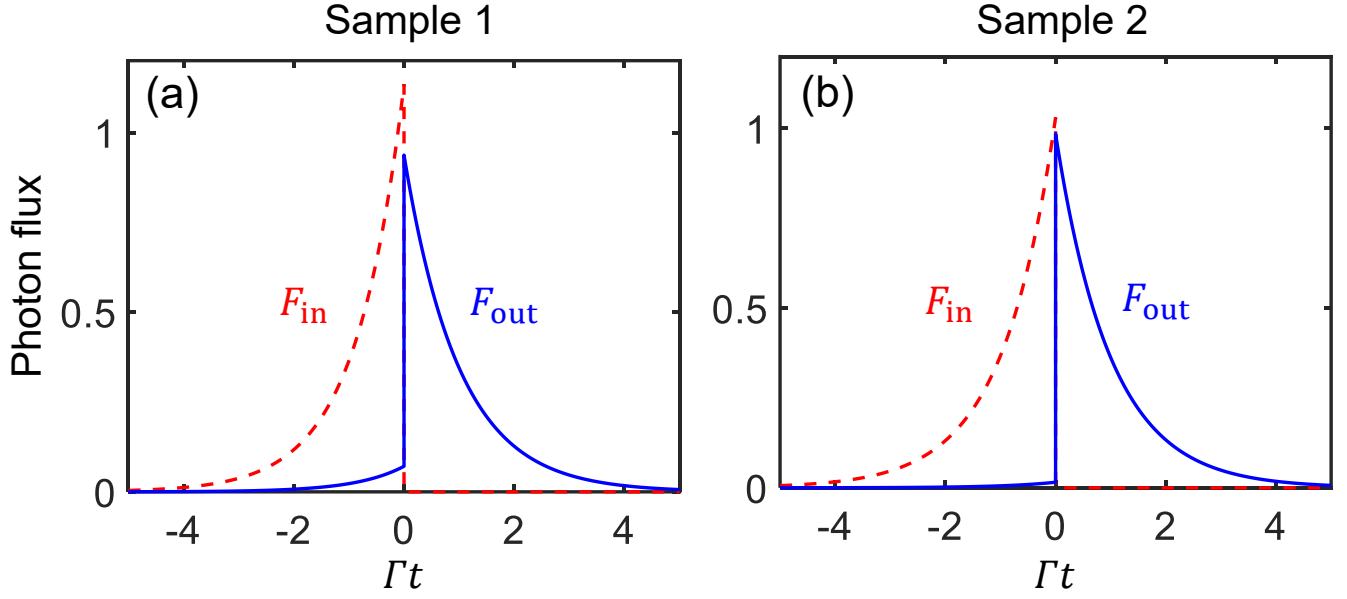


Figure S8. Theory plot of input and output photon flux as functions of time. (a) and (b) correspond to sample 1 and 2 with $\Gamma_{\phi,n} = 0.067\Gamma$ and $\Gamma_{\phi,n} = 0.0152\Gamma$, respectively (see main text). The red dashed curves represent the exponential rising incident flux $F_{\text{in}}(t)$ with $\tau_{\text{opt}} = \sqrt{2/(\gamma\Gamma)}$ and the blue solid curves the resulting output flux $F_{\text{out}}(t)$. The fluxes $F_{\text{in/out}}$ are given in units of Γ^{-1} .

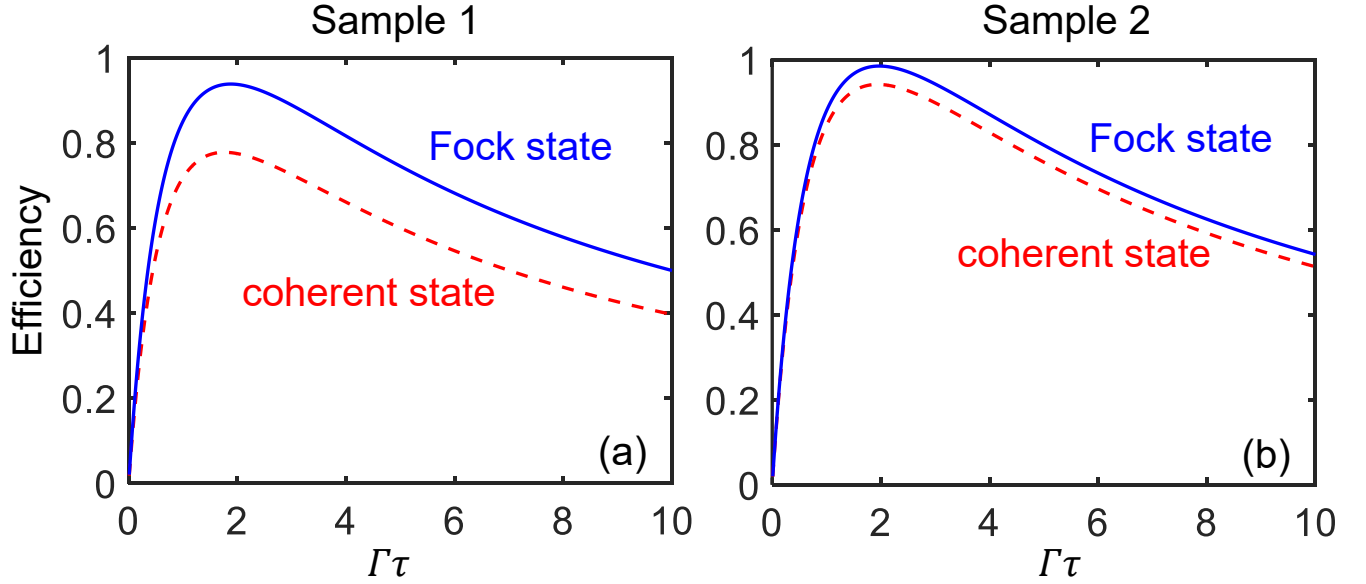


Figure S9. Theory plot of loading efficiency as a function of time constant τ of the exponentially rising input pulse. (a) and (b) correspond to sample 1 and 2, respectively (see main text). The blue (solid) and red (dashed) curves correspond to single-photon Fock-state and coherent-state inputs, respectively.

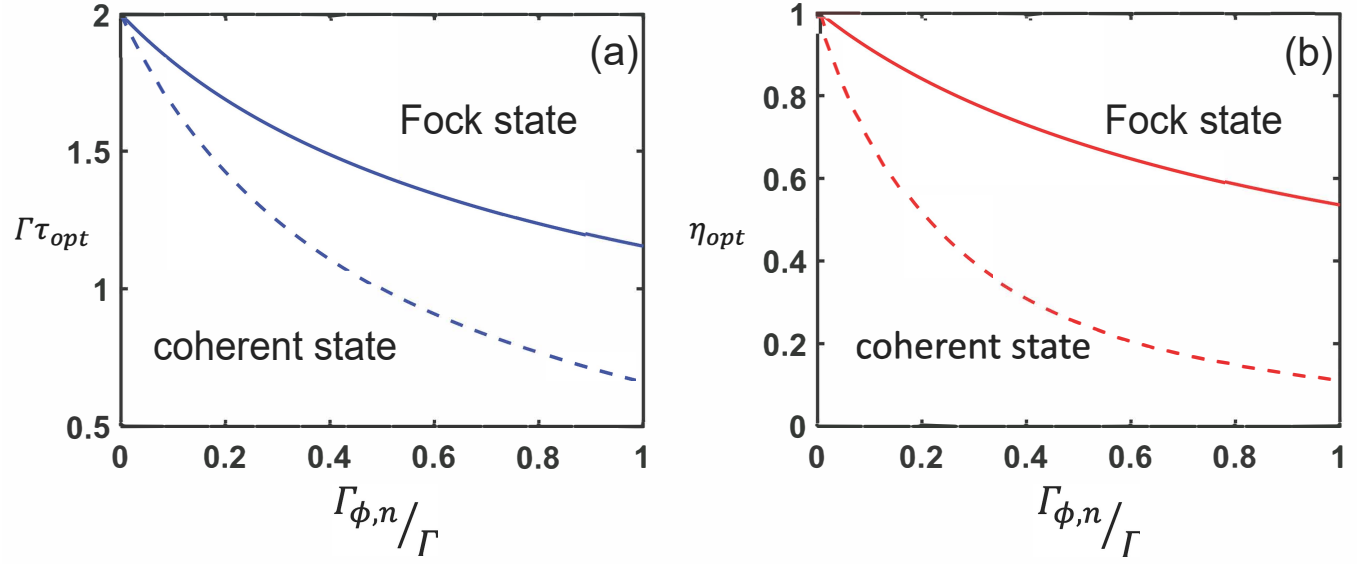


Figure S10. Theory plot of effect of $\Gamma_{\phi,n}$: (a) optimal time constant and (b) loading efficiency as functions of the $\Gamma_{\phi,n}$ with single-photon Fock-state input (solid curves) and weak coherent input (dashed curves).

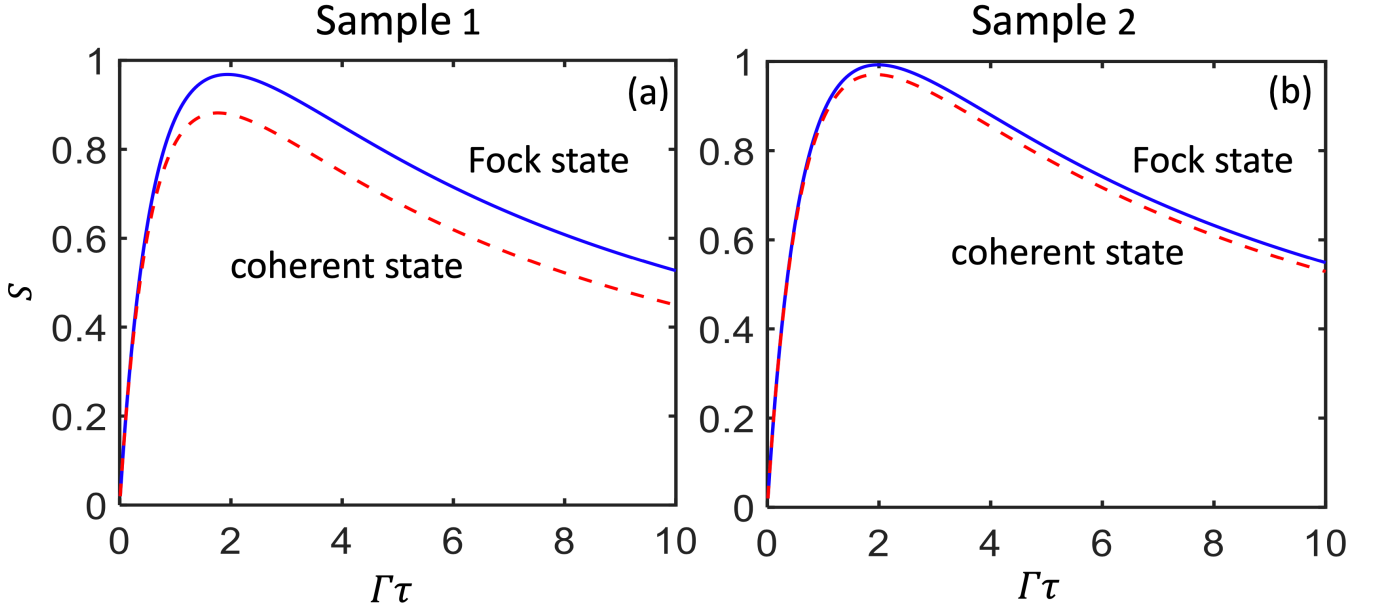


Figure S11. Theory plot of the symmetry factor as a function of time constant τ of the exponentially rising input pulse. (a) and (b) correspond to sample 1 and 2, respectively (see main text). The blue (solid) and red (dashed) curves correspond to single-photon Fock-state and coherent-state inputs, respectively.

S9. TIME-REVERSAL SYMMETRY FOR FOCK-STATE INPUT

In order to reveal the role of time-reversal symmetry between the input and output pulses, we explicitly define a symmetry factor that characterizes the overlap of the temporal waveforms of the input and the time-reversed output signals:

$$S \equiv \frac{\int_{-\infty}^{t_0=0} \sqrt{F_{\text{in}}(t)F_{\text{out}}^{\text{em}}(-t)} dt}{\int_{-\infty}^{t_0} F_{\text{in}}(t) dt}, \quad (\text{S23})$$

where $F_{\text{out}}^{\text{em}}(-t)$ denotes the time-reversed spontaneous-emission photon flux. For single-photon Fock-state inputs, we then obtain

$$S = \sqrt{\frac{32\Gamma^2}{\tau^2(\gamma + 1/\tau)(\Gamma + 2/\tau)^3}} \quad (\text{S24})$$

with $\Gamma = 2\pi g^2(\omega_0)$ maximized at $\tau_{\text{opt}}^S = \left[(\Gamma - 2\gamma) + \sqrt{4\gamma^2 + 28\gamma\Gamma + \Gamma^2} \right] / 8$. We also calculate the symmetry factor for the coherent-state case and find $\tau_{\text{opt}}^S = \tau_{\text{opt}} = 1/\gamma$.

Note that $S \leq 1$; the upper limit corresponds to perfect time-reversal symmetry between the input pulse and the output signal. In the case with $\Gamma_{\phi,n} = 0$, $\tau_{\text{opt}}^S = 2/\Gamma$ also leads to $\eta = 1$. For arbitrary $\Gamma_{\phi,n}$, the condition given by the maximal symmetry factor only differs slightly from that of the maximal loading efficiency. In Fig. S11, we show the symmetry factor as a function of the characteristic time constant τ of the input pulse. We find $S(\tau_{\text{opt}}^S) \approx 96.8\%$ and $\eta \approx 93.8\%$ for sample 1 and $S(\tau_{\text{opt}}^S) \approx 99.3\%$ and $\eta \approx 98.5\%$ for sample 2. We also observe that the symmetry factor is more robust against pure dephasing in the Fock-state cases than in the coherent-state cases.

-
- [S1] I.-C. Hoi, A. F. Kockum, L. Tornberg, A. Pourkabirian, G. Johansson, P. Delsing, and C. M. Wilson, “Probing the quantum vacuum with an artificial atom in front of a mirror,” *Nature Physics* **11**, 1045 (2015), arXiv:1410.8840.
- [S2] Y. Lu, A. Bengtsson, J. J. Burnett, E. Wiegand, B. Suri, P. Krantz, A. F. Roudsari, A. F. Kockum, S. Gasparinetti, G. Johansson, and P. Delsing, “Characterizing decoherence rates of a superconducting qubit by direct microwave scattering,” *npj Quantum Information* **7**, 35 (2021), arXiv:1912.02124.
- [S3] Y. Lu, I. Strandberg, F. Quijandria, G. Johansson, S. Gasparinetti, and P. Delsing, “Propagating Wigner-negative states generated from the steady-state emission of a superconducting qubit,” *Physical Review Letters* **126**, 253602 (2021).
- [S4] Y. Wang, J. Minar, L. Sheridan, and V. Scarani, “Efficient excitation of a two-level atom by a single photon in a propagating mode,” *Physical Review A* **83**, 063842 (2011), arXiv:1010.4661.
- [S5] H. S. Rag and J. Gea-Banacloche, “Two-level-atom excitation probability for single- and N -photon wave packets,” *Physical Review A* **96**, 033817 (2017).
- [S6] M. O. Scully and M. S. Zubairy, *Quantum Optics* (Cambridge University Press, 1997).
- [S7] Y. Wang, J. Minar, and V. Scarani, “State-dependent atomic excitation by multiphoton pulses propagating along two spatial modes,” *Physical Review A* **86**, 023811 (2012).
- [S8] M. J. Collett and C. W. Gardiner, “Squeezing of intracavity and traveling-wave light fields produced in parametric amplification,” *Physical Review A* **30**, 1386 (1984).
- [S9] K. Lalumière, B. C. Sanders, A. F. van Loo, A. Fedorov, A. Wallraff, and A. Blais, “Input-output theory for waveguide QED with an ensemble of inhomogeneous atoms,” *Physical Review A* **88**, 043806 (2013), arXiv:1305.7135.